Carbon 205 (2023) 463–474

Contents lists available at ScienceDirect

Carbon

journal homepage: www.elsevier.com/locate/carbon

Thorough elucidation of synthesis and structure of poly(glycerol) functionalized nanodiamonds

Masahiro Nishikawa [a,b,*], Ming Liu [b], Taro Yoshikawa [b], Hidekazu Takeuchi [b], Naoyoshi Matsuno [b], Naoki Komatsu [a,**]

[a] Graduate School of Human and Environmental Studies, Kyoto University, Sakyo-ku, Kyoto, 606-8501, Japan
[b] Innovation and Business Development Headquarters, Daicel Corporation, 1239, Shinzaike, Aboshi-ku, Himeji, Hyogo, 671-1283, Japan

A B S T R A C T

Poly(glycerol) (PG) is one of the most promising platforms for the surface modification of nanomaterials especially for *in vivo* applications. Since the "grafting-from" process is facile to functionalize the nanomaterial surface covalently through the ring-opening polymerization of glycidol (GD), it has been applied to a variety of nanomaterials. The resulting numerous hydroxy groups in the hyperbranched structure serve as scaffolds for further functionalization and provide good dispersibility under physiological conditions. On the other hand, nanodiamond (ND) is a nanomaterial most intensely worked with PG because of its prominent properties including fluorescence from color centers. Despite the wide-spread use, the process has not been extended to be scalable and controllable. In addition, the structural details of PG chain on ND surface are yet elusive. In this work, we develop more scalable and safer PG functionalization of NDs by dropwise-addition of GD to ethylene glycol (EG) suspension of ND. The resulting PG amount can be controlled or even estimated by the reaction conditions (weights of GD, ND and EG) and the ND properties (diameter and oxygen content). The structure of PG chain was qualitatively and quantitatively analyzed by ^{13}C nuclear magnetic resonance (NMR) and dynamic light scattering (DLS) measurements. Based on these results, the structure of PG is elucidated.

1. Introduction

For practical use of nanoparticles (NPs) such as *in vivo* applications, the dispersibility of NPs in the aqueous environment is essential. Poly (glycerol) (PG) is one of the most promising hydrophilic coatings for NPs due to its hydrophilicity and biocompatibility as well as protein-repellent property [1–3]. Although PG coating has been employed to functionalize the surfaces of various NPs [4–6], we found the direct "grafting-from" process to initiate the ring-opening polymerization of glycidol (GD) directly from the NP surface without any precoating under neutral conditions without any additives. This finding made the reaction process much simpler and the PG coating much denser. The resulting numerous hydroxy groups in PG layer gave high aqueous dispersibility and high extensibility for further functionalization to NPs [7]. While our direct "grafting-from" PG functionalization is found to apply to various NPs such as superparamagnetic iron oxide, boron carbide and titanium oxide NPs [8–10], nanodiamonds (NDs) including detonation ND (DND) and high pressure high temperature ND (HPHT-ND) have been investigated most intensively for their *in vivo* applications for sensing and imaging [11–22], and treatment [23–26]. Actually, several reviews including PG functionalized ND (ND-PG) have been published for the recent two years [7,27–32]. Despite the wide-spread use of the simple process, the "grafting from" methodology has not been extended to be scalable and controllable. In addition, the detailed molecular structure of PG on the ND surface is elusive, though the polymer structure and polymerization mechanism were reported for the PG without any core materials, namely free PG [33–36]. The recent investigation on the colloidal stability of DND-PG also motivated us to elucidate the chemical structure of PG on the surface of NDs [37].

In this work, we developed a PG functionalization process through dropwise addition of GD to ND suspension in ethylene glycol (EG), making the process safer and scalable by keeping the concentration of GD much lower than the previous conditions without solvent during the reaction. The thorough elucidation of the reactions enabled us to control the PG amount for NDs theoretically by the properties of ND (diameter and oxygen content) and the reaction conditions (weights of GD, ND and EG). The chemical structures of these ND-PG were elucidated by ^{13}C NMR measurements using inverse gated decoupling and dynamic light

Abbreviations: PG, Poly(glycerol); ND, nanodiamond; GD, glycidol; EG, ethylene glycol; NMR, nuclear magnetic resonance; DLS, dynamic light scattering; NPs, nanoparticles; DND, detonation nanodiamond; TGA, thermogravimetric analysis; DB, degree of branching.

* Corresponding author. Graduate School of Human and Environmental Studies, Kyoto University, Sakyo-ku, Kyoto, 606-8501, Japan.
** Corresponding author.
E-mail addresses: ma_nishikawa@jp.daicel.com (M. Nishikawa), komatsu.naoki.7w@kyoto-u.ac.jp (N. Komatsu).

https://doi.org/10.1016/j.carbon.2023.01.025
Received 30 September 2022; Received in revised form 5 January 2023; Accepted 10 January 2023
Available online 16 January 2023

scattering (DLS) measurements in various media with different ionic strength. These elucidations should give us an insight for structural design of PG functionalized NPs (NP-PGs) for advanced applications and fundamental understanding of various phenomena of NP-PGs.

2. Results and discussion

2.1. Elucidation of the scalable and controllable synthesis of ND-PG

PG functionalization was employed for four kinds of NDs; DNDs of 4–6 nm in their primary particle sizes with positive and negative ζ-potentials (DND(+) and DND(−), respectively), and HPHT-ND of 50 nm size (ND50) with and without acid treatment (ND50(A) and ND50(N), respectively). DND(+) and DND(−) were prepared by annealing of DND with hydrogen and oxygen, respectively (see details in Experimental) [38,39]. ND50(A) and ND50(N) were prepared from as-received ND50 by treating with a mixture of H_2SO_4 and HNO_3 and by drying to remove adsorbed moisture, respectively. The oxygen contents in these NDs (O_{ND}) were determined by elemental analysis to estimate the number of oxygen-containing functional groups on the surface (Table 1).

In the case of free PG without ND core, it is known that the degree of polymerization is controlled by the ratio between GD and a substrate (alcohol, acid or alkoxide) under homogeneous conditions [33–36]. Although the PG/ND ratio is reported to be controlled in the PG functionalization of ND by the reaction temperature and time [2], the reaction should not be controlled appropriately, as the scale increases, due to the large heat generation by GD (92–109 kJ/mol for a similar epoxy compound [40]). To make the reaction much safer, more scalable and more controllable, we added GD dropwise into DND suspension in EG [26]. EG was used as a solvent because of the high boiling point (197 °C) above the reaction temperature of the PG functionalization and high polarity to dissolve GD and disperse ND-PG (Figs. S1–1), though the starting materials, DND and ND50, were not fully dispersed.

Under the conditions to add GD dropwise to the ND suspension in EG, the PG content was controlled by changing the amounts of GD and EG, and the reaction temperatures to give ten kinds of ND-PG in addition to DND(+) with extrahigh PG content (DND(+)-PG(xh)) prepared under the previous conditions without solvent [24]; DND(+)-PG(xl), -PG(l), -PG(m), -PG(h), DND(−)-PG(l), -PG(m), -PG(h), ND50(N)-PG(l), -PG(m), and ND50(A)-PG where xl, l, m and h denote the extralow, low, medium, and high PG contents, respectively (Table 1). For DND-PGs, the amount of EG (W_{EG}) as a solvent was determined so that the final concentration of DND is 1.6–2 wt%. The final weight of GD over ND weight (W_{GD}/W_{ND}) was adjusted according to the PG content from 0.324 (xl) to 0.833 (xh). The PG/ND weight ratios (W_{PG}/W_{ND}) and PG contents ($W_{PG}/(W_{PG} + W_{ND})$) were determined by thermogravimetric analysis (TGA) shown in Tables 1 and S2-1, and Figs. S2-1 and S2-2. The PG contents are also calculated based on the results of elemental analysis shown in Tables S2-2 and S2-3, giving consistent results with those determined by TGA.

As shown in Fig. 1a, W_{PG}/W_{GD} corresponding to the weight of GD immobilized on the ND surface (W_{PG}) against total amount of GD (W_{GD}) is found to be proportional to W_{GD} against the weight of DND(+) ($W_{DND(+)}$), namely $W_{GD}/W_{DND(+)}$. The larger PG content is obtained in DND(+)-PG(xh) under the previously reported conditions, which are different from those in the reactions for the other DND(+)-PGs. That is, a suspension of DND(+) in GD without EG was reacted at higher temperature, instead of dropwise addition of GD to DND(+) suspension in EG (see the details in Experimental). Surprisingly, the result of DND(+)-PG(xh) is placed on the linear plots drawn by those of the other DND(+)-PGs (blue squares with blue dotted line in Fig. 1a). The following eq. (1) is derived from Fig. 1a and Table 1.

$$W_{PG}/W_{GD} = 0.00110 \times W_{GD}/W_{DND(+)} \quad (1)$$

$$W_{PG} = 0.00110 \times {W_{GD}}^2/W_{DND(+)} \quad (2)$$

The eq. (2) derived from eq. (1) indicates that W_{PG} is proportionate to the square of W_{GD}. This can be interpreted by the reaction mechanism; one GD molecule reacted with PG chain generates two hydroxy groups in either cationic or anionic mechanism (Fig. 2), which can react with two GD molecules to increase W_{PG} quadratically. The eq. (2) also shows that W_{PG} can be determined solely by W_{GD} and $W_{DND(+)}$, not by the concentrations of DND(+) and GD ($W_{DND(+)}/W_{EG}$ and W_{GD}/W_{EG}, respectively) nor by the reaction temperature. These phenomena

Table 1
Summary of ND property, reaction conditions and results in PG functionalization of NDs.

	DND(+)-PG (xl)	DND(+)-PG (l)	DND(+)-PG (m)	DND(+)-PG (h)	DND(+)-PG (xh)	DND(−)-PG (l)	DND(−)-PG (m)	DND(−)-PG (h)
ND (raw material)								
Oxygen content (O_{ND}, x 10^{-2})[a]	5.14	5.14	4.84	4.84	4.84	9.51	9.51	9.51
Reaction conditions								
Ethylene glycol (EG) (W_{EG}/W_{ND})	30.0	30.0	15.0	7.50	–	30.0	30.0	15.0
Glycidol (GD) (W_{GD}/W_{ND})	22.4	30.0	45.0	52.7	65.7	22.5	30.0	45.0
Temperature (°C)	100	100	100	100	140	100	100	100
Results								
PG/ND ratio by TGA (W_{PG}/W_{ND})	0.48	0.99	2.29	2.80	4.99	1.43	1.84	3.62
PG content ($W_{PG}/(W_{PG} + W_{ND})$)	0.324	0.498	0.696	0.737	0.833	0.588	0.648	0.784
Consumption of GD (W_{PG}/W_{GD})	0.0214	0.0330	0.0509	0.0531	0.0760	0.0635	0.0613	0.0804

	ND50(N)-PG(l)	ND50(N)-PG(m)	ND50(A)-PG
ND (raw material)			
Oxygen content (O_{ND}, x 10^{-2})[a]	2.69	2.69	2.92
Reaction conditions			
Ethylene glycol (EG) (W_{EG}/W_{ND})	6.50	6.50	6.84
Glycidol (GD) (W_{GD}/W_{ND})	80	108	107
Temperature (°C)	140	140	140
Results			
PG/ND ratio by TGA (W_{PG}/W_{ND})	0.69	0.85	1.19
PG content ($W_{PG}/(W_{PG} + W_{ND})$)	0.408	0.458	0.542
Consumption of GD (W_{PG}/W_{GD})	0.00861	0.00787	0.0111

[a] Determined by elemental analysis.

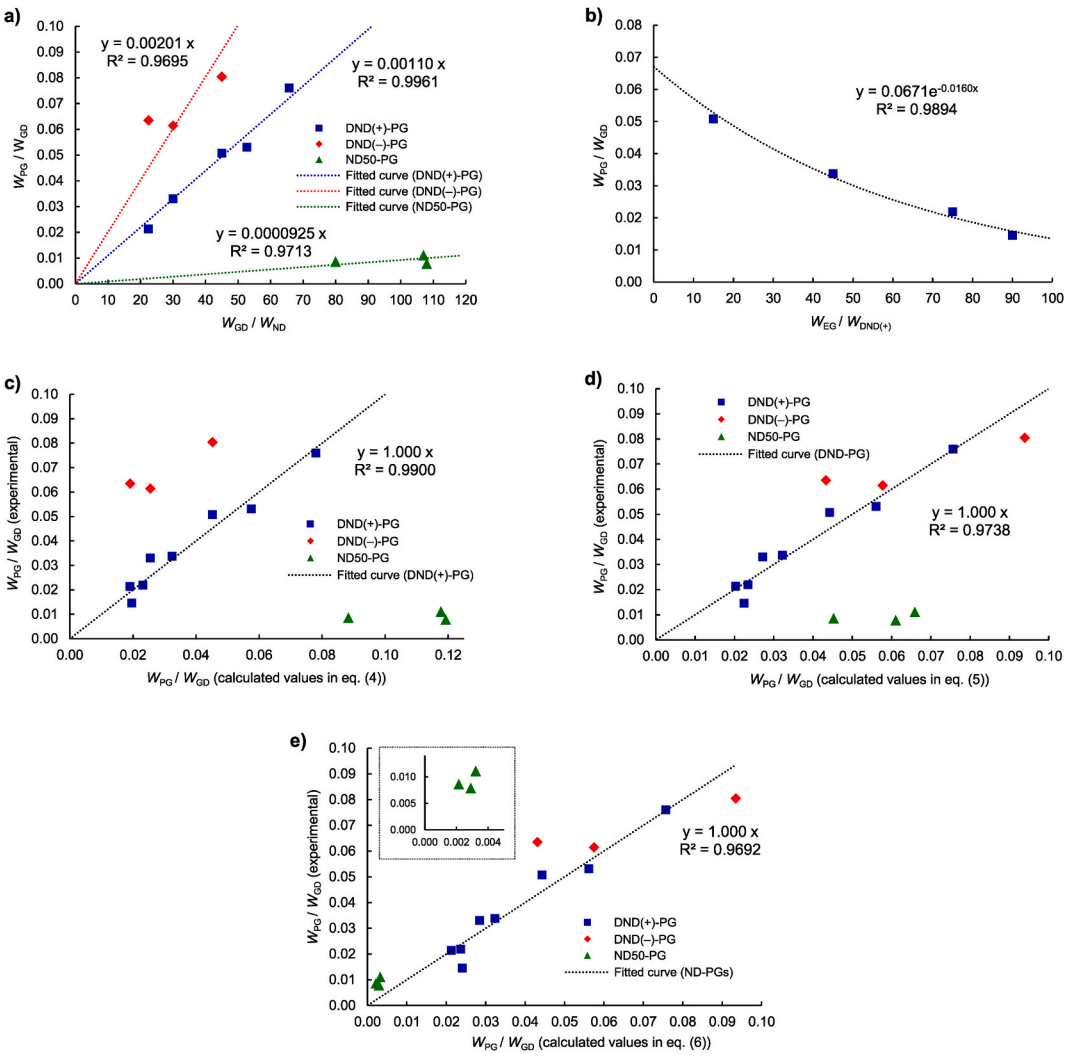

Fig. 1. Relationships of the experimental results (W_{PG}/W_{GD}) with the calculated values from the equations based on the reaction conditions (W_{GD}, W_{EG} and W_{ND}) and the ND properties (O_{ND} and D_{ND}); a) W_{GD} and W_{ND} in eq. (1), b) W_{EG} and $W_{DND(+)}$ in eq. (3), c) W_{GD}, W_{EG} and W_{ND} in eq. (4), d) W_{GD}, W_{EG}, W_{ND} and O_{ND} in eq. (5), and e) W_{GD}, W_{EG}, W_{ND}, O_{ND} and D_{ND} in eq. (6). The inset shows the magnification of the area of ND50-PGs. (A colour version of this figure can be viewed online.)

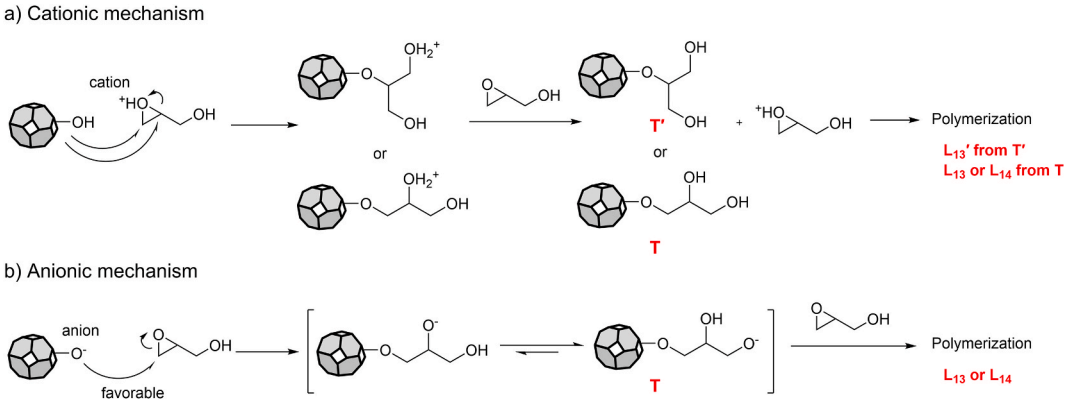

Fig. 2. a) Cationic and b) anionic mechanisms in ring-opening polymerization of GD on ND surface. The red letters stand for the substructures shown in Fig. 3. (A colour version of this figure can be viewed online.)

indicate that the reactions of GD with EG and GD are much slower than those of GD with PG in ND-PG and/or free PG in the reaction mixture. In other words, the hydroxy groups in EG and GD are much less reactive than those in PG. To confirm this experimentally, the reactions under more diluted conditions were conducted in 3, 5 and 6 times larger $W_{EG}/W_{DND(+)}$, corresponding to DND(+)-PG(m)-d1, -d2 and -d3 in Table 2 respectively, than that in DND(+)-PG(m) in Table 1. Based on the PG contents determined by TGA (Tables 2 and S3-1, and Figs. S3–1), $W_{PG}/$

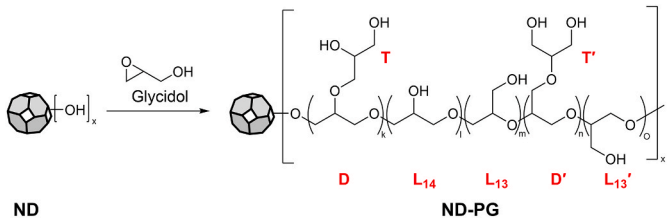

Fig. 3. Substructures in PG chain on ND surface. (A colour version of this figure can be viewed online.)

Table 2
Summary of ND property, reaction conditions and results in PG functionalization of NDs under diluted conditions.

	DND(+)-PG (m)-d1	DND(+)-PG (m)-d2	DND(+)-PG (m)-d3
ND (raw material)			
Oxygen content (O_{ND}, x 10^{-2})[a]	5.14	4.84	4.84
Reaction conditions			
Ethylene glycol (EG) (W_{EG}/W_{ND})	90.0	75.0	45.0
Glycidol (GD) (W_{GD}/W_{ND})	45.0	45.0	45.0
Temperature (°C)	100	100	100
Results			
PG/ND ratio by TGA (W_{PG}/W_{ND})	0.66	0.99	1.52
PG content ($W_{PG}/(W_{PG}+W_{ND})$)	0.396	0.497	0.603

[a] Determined by elemental analysis.

W_{GD} is found to have a negative exponential relationship with $W_{EG}/W_{DND(+)}$ as shown in Fig. 1b and eq. (3). The coefficient (*y*-intercept) corresponds to an extrapolated W_{PG}/W_{GD}, when $W_{EG}/W_{DND(+)}$ is 0.

$$W_{PG}/W_{GD} = 0.0671/e^{0.0160\times W_{EG}/W_{DND(+)}} \quad (3)$$

In eq. (3), the more diluted conditions with increase of $W_{EG}/W_{DND(+)}$ reduces W_{PG}/W_{GD}, meaning that more GD reacts with EG rather than DND(+) under the conditions with the same $W_{GD}/W_{DND(+)}$ (45.0 in Table 2). When W_{PG}/W_{GD} becomes half of the *y*-intercept ($W_{EG}/W_{DND(+)} = 0$), $W_{EG}/W_{DND(+)}$ is 43.3 (ln 2/0.0160), which corresponds to > 430 in the ratio of the oxygen contents between EG (O_{EG} = 52 wt%) and DND(+) ($O_{DND(+)}$ = ~5 wt% in Table 1) in the reaction mixture. This indicates that the reactivity of EG towards GD is much lower than that of DND(+), because ratio of the oxygen contents is assumed as that of the number of oxygen containing functional groups which are the potential reaction sites for GD. Although DND(+) was prepared by heating as-synthesized DND under hydrogen atmosphere followed by bead milling (see Experimental), it still shows the IR absorptions at 1717 and 3109 cm^{-1} corresponding to carbonyl and hydroxy groups, respectively (Fig. S4–1b) as well as ~5 wt% $O_{DND(+)}$ (Tables 1 and S2-2). Therefore, a number of oxygen containing functional groups including hydroxy and carboxylic groups may exist and the ring-opening polymerization of GD may be facilitated by the protons at carboxylic groups on DND(+) surface through cationic mechanism (Fig. 2a). The influence of EG, or concentration of DND(+) in EG ($W_{EG}/W_{DND(+)}$), to W_{PG}/W_{GD} shown in Fig. 1b and eq. (3) is incorporated into the linear relationship between W_{PG}/W_{GD} and $W_{GD}/W_{DND(+)}$ as shown in Fig. 1a (blue dotted line) and eq. (1) to give Fig. 1c (blue squares and dotted line) and eq. (4). The eq. (4) consists of the relationship between $W_{GD}/W_{DND(+)}$ and W_{PG}/W_{GD} in the former part, and the influence by EG in the latter part. Two coefficients, 0.00119 and 0.0111, in eq. (4) are determined by a least-square method to give good correlations with the experimental results (the blue squares and the dotted line in Fig. 1c).

$$W_{PG}/W_{GD} = 0.00119\times\left(W_{GD}/W_{DND(+)}\right)/e^{0.0111\times\left(W_{EG}/W_{DND(+)}\right)} \quad (4)$$

When the ζ-potential of DND turned into negative, W_{PG}/W_{GD} in DND (−)-PG(l), -PG(m) and -PG(h) are 3.0, 1.9 and 1.6 times as large as W_{PG}/W_{GD} in DND(+)-PG(xl), -PG(l) and -PG(m) prepared under the same conditions, respectively (Table 1). This can be attributed to the difference in the oxygen contents (O_{DND}) of DND(+) and DND(−); 5.14 × 10^{-2} and 4.84 × 10^{-2} in $O_{DND(+)}$, and 9.51 × 10^{-2} in $O_{DND(-)}$ (Table 1), because the ring-opening polymerization of GD on the surface of DND is initiated and/or facilitated by the oxygen containing functional groups corresponding to O_{DND}. Although not all the oxygen atoms in DND are involved in the reaction, O_{DND} is incorporated into the former part of eq. (4) as a multiplier. Meanwhile, it is added as a divisor in the exponential part, because the influence of EG relatively decreases as O_{DND} increases. The coefficients 0.0238 and 0.000512 in eq. (5) are determined by a least-square method to give Fig. 1d (blue squares and red rhombi with dotted line), indicating that W_{PG} in DND-PGs can be controlled by O_{DND}, W_{GD}, W_{EG} and W_{DND} irrespective of the ζ-potential of DNDs.

$$W_{PG}/W_{GD} = 0.0238\times(W_{GD}/W_{DND})\times O_{DND}/e^{0.000512\times(W_{EG}/W_{DND})/O_{DND}} \quad (5)$$

Since the diameters of ND50 and DND are determined to be 43.35 and 4.96–5.15 nm which will be mentioned below, specific surface area of DNDs is calculated to be 8.4–8.7 times larger than that of ND50. Since the specific surface area should influence the W_{PG}/W_{GD} in the same direction as the oxygen content, the diameters (D_{ND}), which is inversely proportional to the specific surface area, are incorporated into eq. (5) as a divisor of O_{ND} for both former and exponential parts as shown in eq. (6). The coefficients 0.122 and 0.0000990 are determined in similar manners to those of eq. (4) and eq. (5). Since all the results of DND (+)-PG (blue squares), DND(−)-PG (red rhombi) and ND50-PG (green triangles) are almost on the dotted line as shown in Fig. 1e, it is concluded that W_{PG} in the PG functionalization for any NDs is determined by the properties of ND (diameter and oxygen content) and reaction conditions (weights of GD, ND and EG).

$$W_{PG}/W_{GD} = 0.122\times(W_{GD}/W_{ND})\times(O_{ND}/D_{ND})/e^{0.0000990\times(W_{EG}/W_{ND})/(O_{ND}/D_{ND})} \quad (6)$$

2.2. Structural elucidation of ND-PG by ^{13}C NMR analyses

The PG chain consists of several substructures of glycerol as shown in Fig. 3. On the ring-opening polymerization, 2- and 3-positions of GD (CH and CH_2 in oxirane ring of 2,3-epoxypropan-1-ol, respectively) are subject to nucleophilic attack, giving various structural isomers via two possible reaction mechanisms, cationic and anionic ones shown in Figs. 2a and b, respectively. There are dendritic (D and D′), linear (L_{13}, L_{13}' and L_{14}) and terminal (T and T′) glycerol units having three, two and one ether linkage(s), respectively (Fig. 3). They are also divided into two patterns having ether linkage with the preceding unit at the primary carbon (D, L_{13}, L_{14} and T) and secondary one (D′, L_{13}' and T′). The linear structures including three and two carbons between the ether linkages are L_{14} unit, and L_{13} and L_{13}' units, respectively. Hereafter, L_{13} includes L_{13}' unless otherwise specified, since these two substructures are indistinguishable each other in ^{13}C NMR.

To elucidate the structures in PG on ND quantitatively, solution phase ^{13}C NMR (Fig. 4) was measured by inverse gated decoupling experiment with repetition time of 8 s which is more than 10 times as long as the T_1 relaxation time shown in Supporting Information S5. As shown in our previous papers, a broad signal from diamond core is detected and set at 36.3 ppm as a reference [1,41]. The signals of PG chain were assigned by DEPT, HMQC and HMBC spectra described in detail in Supporting Information S6 and by previously reported ^{13}C NMR spectra of free PG [33–36]. The peak assignments and relative integration values are shown in Table 3 and Fig. S7–1. Since the separation of two signals at 73.0 and 72.7 ppm, and 71.4 and 71.1 ppm are not enough, they are treated as one peak.

First, the integral ratio between PG and ND (I_{PG}/I_{ND}) leads to their weight ratio (W_{PG}/W_{ND}) by dividing them with their carbon contents, C_{PG} and C_{ND}, according to eq. (7).

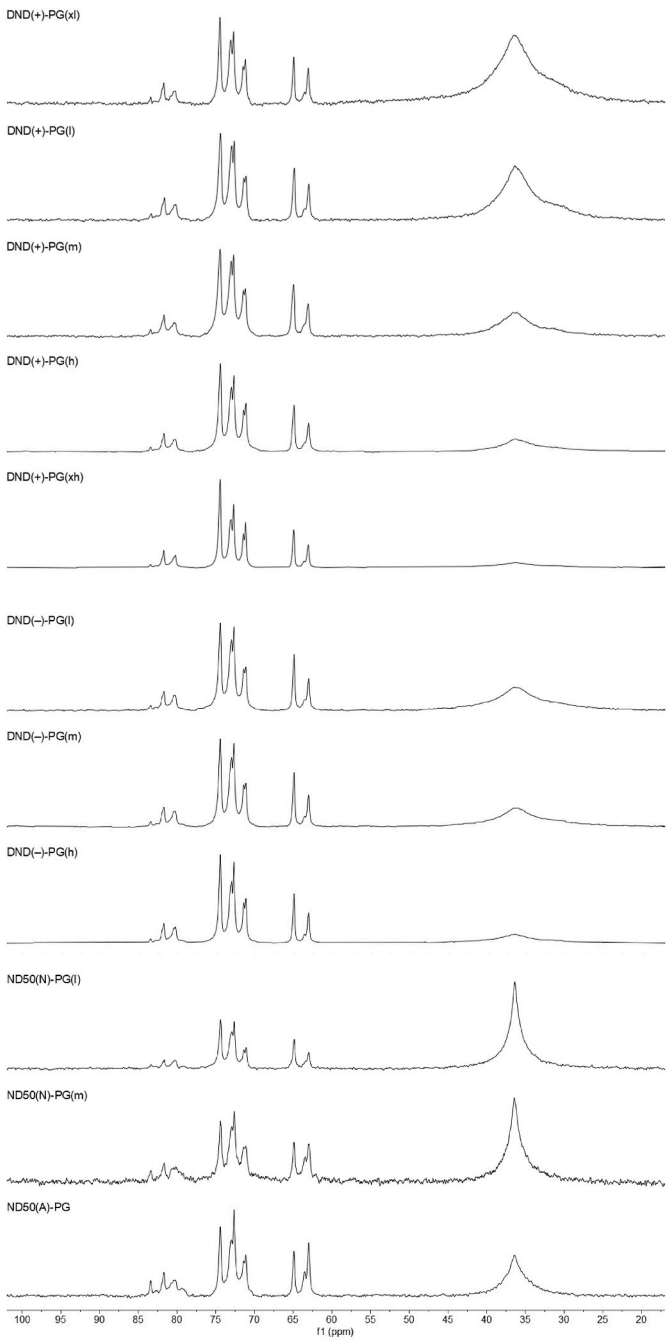

Fig. 4. ^{13}C NMR spectra of ND-PGs in D_2O. Chemical shift of the peak top of diamond core is adjusted to 36.3 ppm as a reference.

$$W_{PG} / W_{ND} = (I_{PG}/C_{PG}) / (I_{ND}/C_{ND}) \quad (7)$$

The W_{PG}/W_{DND} determined by ^{13}C NMR (Table 3), namely $(W_{PG}/W_{DND})_{NMR}$, exhibits a linear relationship with that determined by TGA (Table 1), namely $(W_{PG}/W_{ND})_{TGA}$, as shown in Fig. 5a and eq. (8).

$$(W_{PG}/W_{DND})_{NMR} = 1.808 \times (W_{PG}/W_{DND})_{TGA} - 0.529 \quad (8)$$

The slope of 1.808 implies that approximately 55% of the carbon atoms in the DND core (DND carbons) in DND-PGs are detected by ^{13}C NMR, because it should be 1.0 when all the DND carbons are detected. The undetected DND carbons (approximately 45%) may be included in disordered carbon layer near the surface and/or deep inside the core [42,43]. The negative *y*-intercept shown in Fig. 5a indicates that some of the carbon atoms in PG layer (PG carbons) are not detected by ^{13}C NMR probably due to the motility inhibition of these PG carbons near the DND surface. The undetected PG carbons are calculated to be 29 wt% at $(W_{PG}/W_{DND})_{TGA}$ from the *x*-intercept at $(W_{PG}/W_{DND})_{NMR} = 0.0$ in Fig. 5a and eq. (8). The excellent linearity ($R^2 > 0.99$) means that the PG carbons detected by ^{13}C NMR in weight or number are strictly proportional to the PG content determined by TGA regardless of the electrical potential of DND. Hereafter, the detailed structures of DND-PGs will be discussed quantitatively based on the integration values of the carbon atoms detected by inverse gated decoupling measurement.

A similar relationship is observed in ND50-PGs as shown in Fig. 5b and eq. (9), where ND50-PG shows the larger slope and larger negative *y*-intercept than DND-PG. They indicate that only about 24 wt% of the ND50 carbons are detected by ^{13}C NMR due to much larger diameter than DND, and that 44 wt% of the PG carbons are undetected probably due to larger PG carbon content near the ND50 surface.

$$(W_{PG}/W_{ND50})_{NMR} = 4.210 \times (W_{PG}/W_{ND50})_{TGA} - 1.854 \quad (9)$$

Next, the contents of the substructures in PG chain are discussed based on their relative abundance determined by the formulas shown in Table 4. As the signals in lower magnetic field (85–80 ppm) are split with low signal/noise (S/N) ratio, the integration values in this region are not used. The results are shown in Table 5. The degree of branching (DB) is determined by eq. (10), representing the reactivity of hydroxy groups in the ring-opening polymerization.

$$DB = 2D / (2D + L_{13} + L_{14}) \quad (10)$$

DB should be between 0.0 for linear structure and 1.0 for complete dendritic structure. It would be around 0.5, if the ring-opening reaction of GD, or the chain extension of PG, happens at the all the hydroxy groups at equal possibility [33,44]. As shown in Table 5, DB values of DND-PGs range from 0.47 to 0.58 which are in the same range as that of free PG, indicating that steric and electrostatic effects of DND is negligible in the ring-opening polymerization on DND surface. This supports the above assumption of almost the same reactivity of the PG layer with or without ND core.

As for the contents of the substructures, L_{13} and L_{14} in the DND-PG are found to linearly correlate with the W_{PG}/W_{DND} as shown in Fig. 6. ^{1}H NMR spectra also support the relationship qualitatively (Fig. S7–2); the signal height at 4.11 ppm corresponding to 2-position of L_{14} substructure (−C<u>H</u>(OH)−) increases according to the increase of W_{PG}/W_{DND}. This phenomenon can be interpreted by the reaction mechanism of the oxirane ring opening in GD (Figs. 2a and b). In cationic mechanism, the nucleophilic attack at 2-position leading to L_{13}' and T′ is considered to happen more frequently than that to 3-position, because the carbon at 2-position is more electrophilic than that at 3-position (Fig. 2a). In contrast, the nucleophilic attack at the 3-position of GD leading to L_{14} is favored more than that at the 2-position leading to L_{13}' in anionic mechanism, because the steric hindrance become larger at the higher W_{PG}/W_{DND} (Fig. 2b). There may be a contribution of cationic mechanism in DND-PGs judging from the fact of the existence of T′ substructure, which is characteristic of the cationic mechanism [35,36]. The higher L_{13} abundance must be due to the contribution of L_{13}' derived from T′ structure. The observation in Fig. 6 under the circumstances can be interpreted that the nucleophilic attack at 3-position is facilitated by the steric hindrance increasing along with the extension of PG chain, making the L_{14} abundance larger.

The contents of the substructures (Table 5) are also correlated with those of primary and secondary hydroxy groups. Since the primary hydroxy groups are in T, T′ and L_{13} substructures, their contents are calculated to be 49–58% for DND-PGs and 66–77% for ND50-PGs out of the total hydroxy groups, and 28–53% and 32–58%, respectively, for hydroxy group in ^{13}C NMR detectable PG layer (Table 6). In terms of the further chemical modification, the higher abundance of primary hydroxy group especially in ^{13}C NMR detectable PG layer would be preferable.

Table 3
Signal assignments of ^{13}C NMR of ND-PG and relative integration values of each peak by inverse gated decoupling experiments.

Chemical shift (ppm)[a]	Assignment	Relative integration values of PG chain signals							
		DND(+)-PG (xl)	DND(+)-PG (l)	DND(+)-PG (m)	DND(+)-PG (h)	DND(+)-PG (xh)	DND(−)-PG (l)	DND(−)-PG (m)	DND(−)-PG (h)
83.4	T′	1.47	2.05	1.61	1.03	1.05	1.17	1.26	1.35
81.7	L_{13}[b]	5.46	5.52	5.01	4.77	4.64	4.67	4.68	4.73
80.2	D (D′)	5.62	6.05	4.89	4.87	5.94	5.79	6.79	7.15
74.4	L_{14}, T	23.15	23.53	24.47	24.58	25.52	23.43	22.71	22.68
73.0, 72.7	T, D, L_{14}	31.21	30.22	30.63	30.61	30.79	32.39	32.06	31.96
71.4, 71.1	L_{13}[b], L_{14}	14.75	14.14	15.51	16.59	16.34	14.63	14.88	15.39
64.9	T	9.13	9.74	9.94	9.60	8.51	9.80	9.67	9.02
63.6	T′	2.12	2.05	1.61	1.89	1.62	2.21	1.93	1.77
63.1	L_{13}[b]	7.09	6.69	6.33	6.07	5.59	5.92	6.03	5.93
36.3	DND core[c]	278.0	148.7	58.16	38.91	21.16	80.74	62.23	28.76
$(W_{PG}/W_{DND})_{NMR}$		0.65	1.21	3.17	4.74	8.71	2.08	2.70	5.84

Chemical shift (ppm)[a]	Assignment	Relative integration values of PG chain signals		
		ND50(N)-PG(l)	ND50(N)-PG(m)	ND50(A)-PG
83.4	T′	1.66	3.79	3.25
81.7	L_{13}[b]	4.14	5.56	5.33
80.2	D (D′)	6.08	10.61	9.86
74.4	L_{14}, T	23.76	15.15	15.27
73.0, 72.7	T, D, L_{14}	32.60	28.28	30.26
71.4, 71.1	L_{13}[b], L_{14}	12.16	13.89	13.82
64.9	T	11.19	7.58	7.77
63.6	T′	2.35	5.56	5.06
63.1	L_{13}[b]	6.08	9.60	9.49
36.3	ND50 core[c]	186.74	112.88	61.97
$(W_{PG}/W_{ND50})_{NMR}$		1.05	1.73	3.15

[a] Chemical shift at peak-top of each signal.
[b] L_{13} includes L_{13}'.
[c] The value when the sum of the values of PG carbon is 100.

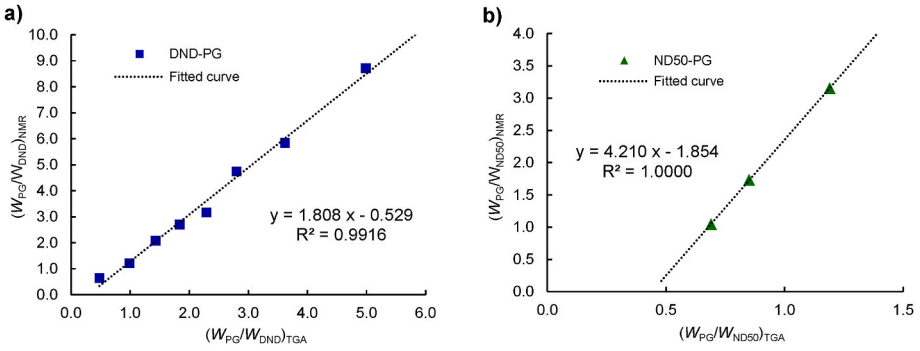

Fig. 5. Relationship in a) PG/DND and b) PG/ND50 weight ratios between TGA ($(W_{PG}/W_{ND})_{TGA}$) and ^{13}C NMR integration values ($(W_{PG}/W_{ND})_{NMR}$). DND and ND50 include a) DND(+) and DND(−), and b) ND50(N) and ND50(A), respectively. (A colour version of this figure can be viewed online.)

Table 4
Formulas to obtain the amount of substructures.

Substructure	Calculation formula for each substructure[a]
T	$I_{64.9} \times 3/2$
T′	$I_{63.6} \times 3$
L_{13}	$I_{63.1} \times 3$
L_{14}	$(I_{71.4\ and\ 71.1} - I_{63.1}) \times 3$
D	$\{I_{73.0\ and\ 72.7} + I_{74.4} - 2 \times (I_{71.4\ and\ 71.1} - I_{63.1}) - 2 \times I_{64.9}\} \times 3/2$

[a] I_x: Integration value of peak at x ppm.

2.3. Structural elucidation of ND-PG by DLS measurements

The thickness of PG layer is calculated from the difference between the hydrodynamic diameter of ND-PG determined by DLS and the ND core size. The DLS of ND-PG was measured in water and 10 mM NaCl, since it has been reported that ionic strength of the medium affects the behavior of ND-PG in dispersion [37]. Among the data processing on number, volume and intensity (scattered light intensity) bases, the number basis is adopted for discussion.

To determine the sizes of ND-PGs, we first investigated their concentration dependence on the DLS size as shown in Fig. 7. DLS results were not corrected by the viscosity of dispersion, since no significant change in viscosity was observed in the concentration range of 0.1–1.0% (Table S8–1). A significant concentration dependence is observed in both DND(+)-PG(m) and ND50(A)-PG in water. ND-PGs with higher concentration exhibits smaller size as shown in Figs. 7a and c, while ND-PGs in 10 mM NaCl show almost no concentration dependence (Figs. 7b and d). This discrepancy can be interpreted by the difference in dispersion state with different ionic strengths. In the literature [37], the cryogenic transmission electron microscopy (Cryo-TEM) analysis

Table 5
Relative abundance of substructures in PG chain[a] and degree of branching (DB)[b].

Substructure	Relative abundances (%) and DB							
	DND(+)-PG(xl)	DND(+)-PG(l)	DND(+)-PG(m)	DND(+)-PG(h)	DND(+)-PG(xh)	DND(−)-PG(l)	DND(−)-PG(m)	DND(−)-PG(h)
T	25.1	27.3	28.0	27.0	24.1	27.2	27.4	25.8
T′	5.8	5.8	4.5	5.3	4.6	6.1	5.5	5.1
L_{13}	19.5	18.8	17.8	17.1	15.8	16.4	17.0	16.9
L_{14}	21.1	20.9	25.9	29.6	30.4	24.2	25.1	27.0
D	28.6	27.2	23.8	21.0	25.1	26.1	25.1	25.2
DB	0.58	0.58	0.52	0.47	0.52	0.56	0.54	0.53

Substructure	Relative abundances (%) and DB		
	ND50(N)-PG(l)	ND50(N)-PG(m)	ND50(A)-PG
T	30.6	20.5	20.8
T′	6.4	15.1	13.6
L_{13}	16.6	26.0	25.4
L_{14}	16.6	11.6	11.6
D	29.8	26.7	28.6
DB	0.64	0.59	0.61

[a] Total amount of all the substructures in each ND-PG is 100.
[b] DB is calculated by eq. (10).

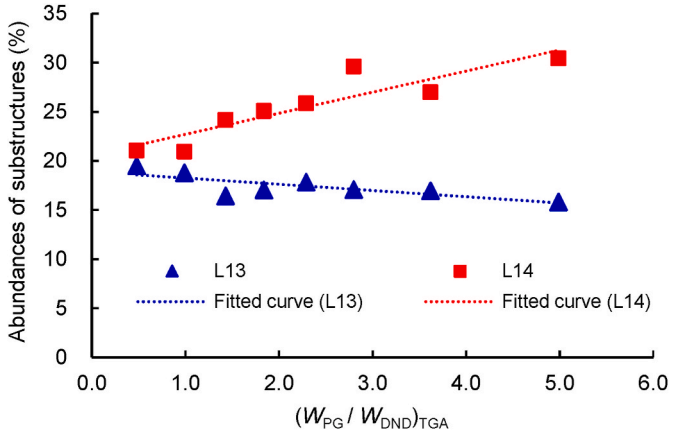

Fig. 6. Abundance in L_{13} and L_{14} substructures in DND-PGs (DND(+) and DND(−)) at various $(W_{PG}/W_{ND})_{TGA}$. (A colour version of this figure can be viewed online.)

reveals that DND-PG tends to form aggregates at lower ionic strength (10^{-7} M), rather than higher one (10^{-2} M), in water likely due to the electrostatic interaction. As the particle concentration increases, the diffusion coefficient increases with the increase of volume fraction, resulting in the decrease of hydrodynamic diameter according to the Stokes-Einstein equation [45]. At higher concentration especially in water, the cooperative diffusion due to diffusion inhibition and the rotational diffusion of non-spherical aggregates may be observed as well as the translation diffusion of single spherical particles that leads the larger diffusion coefficient [46]. The values are approaching to those in 10 mM NaCl (about 72 nm in Fig. 7d) according to the decrease of concentration in ND50(A)-PG due to decrease in the diffusion coefficients (Fig. 7c). Similar phenomena were observed in DND(+)-PG(m) shown in Figs. 7a and b, though the value becomes unstable at the concentration too low (<0.016% in water) to obtain sufficient scattered light intensity. From these observations, the DLS sizes in 10 mM NaCl at 0.10% concentration of ND core were adopted for the actual sizes of ND-PGs as shown in Fig. 8 and Table 7. DLS results of DND- and ND50-PGs in water, 10 mM NaCl and PBS (phosphate buffered saline, pH 7.4 including 137 mM NaCl) are summarized in Fig. S8–1 and Table S8–2, where the dispersions are confirmed to be stable.

To determine the ND size, NDs before PG functionalization were analyzed by DLS in water as shown in Fig. S8–2. DND(+) and DND(−) exhibit the concentration dependence even at the low concentrations such as 0.016 and 0.031%, respectively. The DLS sizes at these low concentrations, 32.16 and 25.11 nm, are much larger than the sizes evaluated by transmission electron microscopy (TEM) probably due to the strong electrostatic interaction [37]. The sizes of DNDs were therefore determined by BET specific surface area (BET-SSA) to be 5.12 and 4.96 nm for DND(+) (2 different lots) and 5.15 nm for DND(−) (Tables 7 and S9-1). On the other hand, the size of ND50 was determined to be 43.35 nm by DLS at the low concentrations of 0.063–0.008% (Table 7 and Fig. S8–2), although the concentration dependence was observed at higher concentrations. Contrary to the case of DNDs, the calculated diameter of ND50 from BET-SSA is 21.1–20.4 nm (2 samples, Table S9–1), which seems to be much smaller than the diameters of commercial ND50 in microscopic images shown in previous reports [47–50]. It would be due to the non-spherical shape of crashed HPHT diamond, or existence of cracks and defects, whereas DNDs are almost spherical shape.

Based on the above results in the sizes of ND-PGs and NDs (Table 7), the lengths of PG chain on NDs are estimated; 5.34–11.44 nm for DND(+)-PG(xl) to DND(+)-PG(xh) corresponding to 11–24 generations, and 5.7–14.60 nm for ND50-PGs corresponding to 13–31 generations, if the length of the one glycerol unit is assumed to be 0.47 nm (Table 7). On the other hand, the calculated numbers of glycerol unit based on the DB of 0.47–0.64 (Table 5) exceed those determined experimentally if all PG chains on the surface have the full generations; 11–24 for DND(+)-PGs and 13–31 for ND50-PGs (Table 7). This indicates that the PG chains shorter than these generations should exist on the surface, probably because the chain growth may be restricted by the adjacent longer chains. Meanwhile, theoretical thickness of PG layer in each ND-PG is calculated from the TGA results on the premise that the PG layer densely covers the ND surface without void space. Assuming the density of PG layer to be 1.261 g/cm^3 (the density of glycerol), the thicknesses of PG layer and the diameter of ND-PGs are calculated to be 0.81–3.74 nm and 6.57–12.60 nm for DND-PGs, and 9.29–13.58 nm and 61.93–70.51 nm for ND50-PGs as shown in Table 8.

The PG layer determined above by DLS (Table 7) are 3–7 times as thick as that calculated from the TGA results in DND-PG, but they are matched in ND50(N)-PG(m) and ND50(A)-PG. In ND50(N)-PG(l), the theoretical thickness of PG layer was larger than the DLS result, but it can be said that the trend is the same as former two results. The difference indicates that the PG layer on the DND is flexible and swells with water to expand their DLS sizes in the aqueous dispersion, while the PG on ND50s did not change their shapes in aqueous solutions due to their strong intra- and/or inter-polymer chain interactions in a dense and

Table 6
Amounts of hydroxy groups in PG layer in various ND-PGs.

	Amount of GD unit and hydroxy group in 1 g of DND-PG							
	DND(+)-PG (xl)	DND (+)-PG(l)	DND(+)-PG (m)	DND(+)-PG (h)	DND(+)-PG (xh)	DND (−)-PG(l)	DND(−)-PG (m)	DND(−)-PG (h)
Hydroxy group in whole PG layer (mmol/g)[a]	4.37	6.72	9.40	9.95	11.24	7.94	8.75	10.58
Hydroxy group in ^{13}C NMR detectable PG layer (mmol/g)[a]	2.16	5.56	9.00	9.65	11.13	7.19	8.21	10.38
Primary hydroxy group in whole PG layer (mmol/g)[b]	2.46	3.88	5.16	5.44	5.51	4.43	4.84	5.59
Primary hydroxy group in ^{13}C NMR detectable PG layer (mmol/g)	1.21	3.20	4.94	5.28	5.45	4.02	4.54	5.49
Content of primary hydroxy group (%)	56.2	57.7	54.9	54.7	49.0	55.9	55.3	52.9
Content of primary hydroxy group in ^{13}C NMR detectable PG layer (%)	27.7	47.7	52.6	53.1	48.5	50.5	51.9	51.8

	Amount of GD unit and hydroxy group in 1 g of ND50-PG		
	ND50(N)-PG(l)	ND50(N)-PG(m)	ND50(A)-PG
Hydroxy group in whole PG layer (mmol/g)[a]	5.51	6.18	7.32
Hydroxy group in ^{13}C NMR detectable PG layer (mmol/g)[a]	2.70	3.93	5.79
Primary hydroxy group in whole PG layer (mmol/g)[b]	3.63	4.74	5.37
Primary hydroxy group in ^{13}C NMR detectable PG layer (mmol/g)	1.78	3.01	4.24
Content of primary hydroxy group (%)	65.9	76.7	73.4
Content of primary hydroxy group in ^{13}C NMR detectable PG layer (%)	32.3	48.7	58.0

[a] Equivalent of the amount of glycerol unit (hydroxy groups on ND surface are not accounted).
[b] Assuming that the ^{13}C NMR undetectable part has the same substructure abundances as the ^{13}C NMR detectable part.

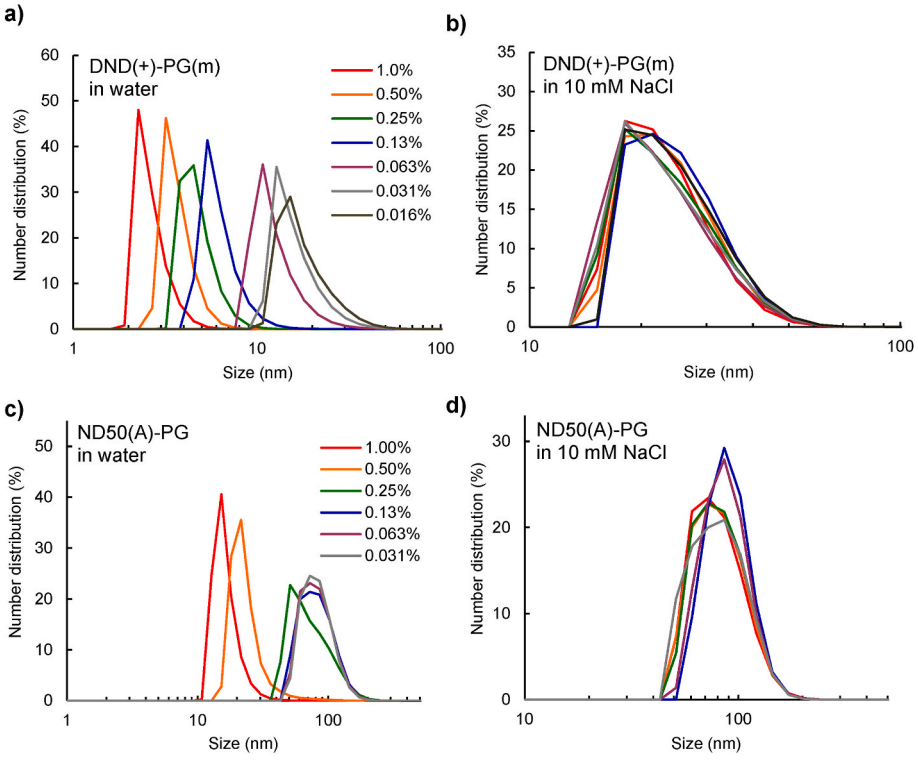

Fig. 7. Concentration dependence of DLS results of a, b) DND(+)-PG(m) and c, d) ND50(A)-PG in a, c) water and b, d) 10 mM NaCl on number basis. The concentrations are based on the ND core. (A colour version of this figure can be viewed online.)

rigid structure. Due to the radial spatial extension on DND particle with higher curvature, a void space between the individual PG chains may be larger than ND50, which can make PG chains more flexible and accommodate more ionic species to dissociate the strong interaction between the chains. In ND50s, the PG chain packs more with less void space due to the smaller curvature.

The above discussion is supported by the relationship of W_{PG}/W_{ND} by TGA with the volume ratio of the expanded structure in 10 mM NaCl to the calculated compact structure (Fig. 9). DND-PGs of higher W_{PG}/W_{ND} have the lower volume ratio, indicating that the density of PG chain becomes higher in DND-PG as W_{PG}/W_{ND} becomes higher. When the ring-opening polymerization proceeds to increase the diameter, the curvature of the particle decreases the resulting less spatial extension and higher density of PG layer in the expanded structure. The increase of

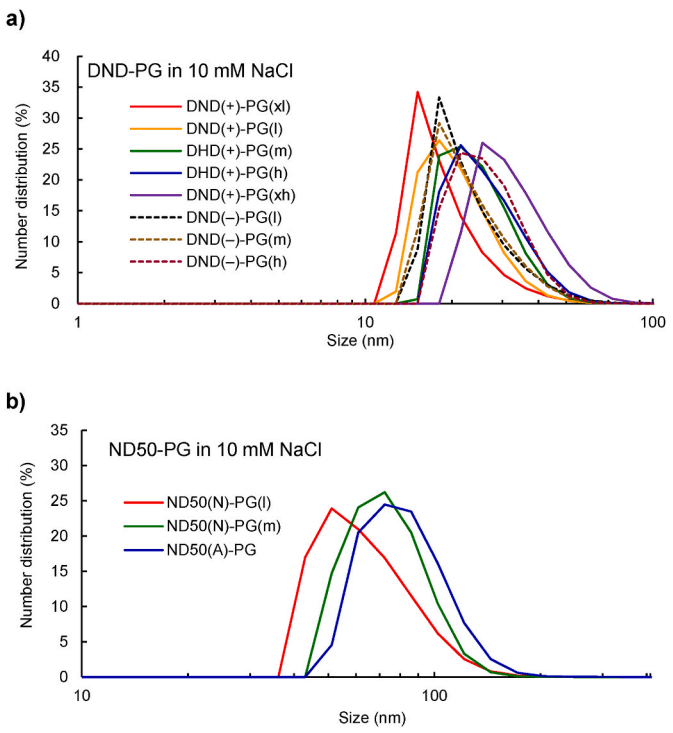

Fig. 8. DLS results of a) DND-PG and b) ND50-PG at ND concentrations of 0.10% in 10 mM NaCl on number basis. (A colour version of this figure can be viewed online.)

density may relate to the increase of abundance of sterically favored L_{14} substructure suggested by ^{13}C NMR described above. In addition, DND-PGs from bare DND with higher oxygen content give higher density of PG chain.

3. Conclusions

We develop a scalable process for PG functionalization of ND using EG as a solvent along with dropwise-addition of GD, making the ring-opening polymerization of GD safely. DND-PGs and ND50-PGs with various PG/ND ratios (W_{PG}/W_{ND}) are prepared under various conditions. After thorough elucidation of the reaction, it is found that the PG amount on ND surface (W_{PG}) can be theoretically controlled by the properties of ND, the diameter and the oxygen content of ND core (D_{ND} and O_{ND}, respectively), and the reaction conditions, the weights of GD, ND and EG (W_{GD}, W_{ND} and W_{EG}, respectively). In ^{13}C NMR analysis of the resulting ND-PGs, we estimate the substructure abundances of the monomer (glycerol) units, implying that cationic mechanism is preferable in the ring-opening reaction of GD. DLS measurement is also performed to determine the thickness of PG layer and the length of PG chain in 10 mM NaCl, where the more reliable data are obtained than those in the other solvents. In addition, the differences in the sizes determined by DLS and calculated by TGA indicate that the PG chain in DND-PG might be flexible to swell with water in aqueous dispersion probably due to the higher curvature of DND.

The results presented here should provide useful information for the quantitative design of further chemical functionalization of ND-PGs especially for biomedical application. For example, the substructure abundance would be important for a regioselective and stoichiometric control of the reaction. In addition, the size information may provide new insights for *in vivo* behavior of the ND-PGs.

4. Experimental

4.1. Materials

DNDs were manufactured by Daicel Corporation (DINNOVARE™). ND50 was purchased from Tomei Diamond Corporation. Hydrochloric acid, 2,3-epoxypropan-1-ol (GD) and ethylene glycol for PG functionalization, and sodium chloride and 10x phosphate-buffered saline (10x D-PBS(−)) for DLS measurement were purchased from FUJIFILM Wako Pure Chemical Corporation (Osaka Japan). D_2O for ^{13}C and ^{1}H NMR measurement was purchased from Tokyo Chemical Industry Co., Ltd. (Tokyo Japan).

4.2. Equipment

^{13}C and ^{1}H NMR spectra were measured by ECX500 NMR spectrometer (JEOL). FT-IR spectra were recorded on IR Tracer-100 FT-IR spectrometer (Shimadzu) equipped with DiffusIR DRIFT chamber (PIKE Technologies). Elemental analyses were conducted at Organic Elemental Microanalysis Center of Kyoto University. Thermogravimetric analysis (TGA) was performed with TG/DTA 6200 (SII). DLS measurement was done by Nanotrac Wave II particle size analyzer (MicrotracMRB). Specific surface area was measured by Belsorp mini-II (Microtrac BEL Corporation). Viscosity was measured by EMS-1000 electro magnetically spinning viscometer (Kyoto Electronics).

4.3. Water dispersion of ζ-positive DND (DND(+))

DND powder was annealed in H_2/N_2 (2/98 (v/v)) at 550 °C for 2 h. Resulting powder was suspended in water (3.0%) and pH was adjusted to 3.5, and then agitated vigorously with ZrO_2 beads (30 μmφ) at the tip speed of 8 m/s for 2 h. ZrO_2 beads were removed by decantation and then, centrifuged at 20000*g* for 10 min to give black dispersion. The

Table 7
PG chain length calculated from the DLS results in 10 mM NaCl.

	DND(+)-PG (xl)	DND(+)-PG (l)	DND(+)-PG (m)	DND(+)-PG (h)	DND(+)-PG (xh)	DND(−)-PG (l)	DND(−)-PG (m)	DND(−)-PG (h)
DLS size in 10 mM NaCl (nm)	15.64	18.09	21.52	22.50	28.00	18.99	19.21	23.11
Diameter of ND core (nm)	4.96[a]	4.96[a]	5.12[a]	5.12[a]	5.12[a]	5.15[a]	5.15[a]	5.15[a]
Thickness of PG layer (nm) [c]	5.34	6.57	8.20	8.69	11.44	6.92	7.03	8.98
Numbers of generation of PG [d]	11.4	14.0	17.4	18.5	24.3	14.7	15.0	19.1

	ND50(N)-PG(l)	ND50(N)-PG(m)	ND50(A)-PG
DLS size in 10 mM NaCl (nm)	55.61	65.40	72.54
Diameter of ND core (nm)	43.35 [b]	43.35 [b]	43.35 [b]
Thickness of PG layer (nm) [c]	6.13	11.03	14.60
Numbers of generation of PG [d]	13.0	23.5	31.1

[a] Calculated from BET-SSA.
[b] DLS result in water at highly diluted condition.
[c] (DLS size in 10 mM NaCl − Diameter of DND core)/2.
[d] Assuming that the length of GD unit is 0.47 nm.

Table 8
Calculated thickness of PG layer in compact structure from the TGA results.

	DND(+)-PG (xl)	DND(+)-PG (l)	DND(+)-PG (m)	DND(+)-PG (h)	DND(+)-PG (xh)	DND(−)-PG (l)	DND(−)-PG (m)	DND(−)-PG (h)
PG/ND ratio by TGA	0.48	0.99	2.29	2.80	4.99	1.43	1.84	3.62
Weight of PG layer (x 10^{-18} g/particle)	0.107	0.221	0.565	0.690	1.230	0.357	0.460	0.904
Volume of PG (nm^3) [a]	84.9	175.1	447.8	547.5	975.7	283.3	364.5	717.1
Volume of ND core (nm^3)	63.7	63.7	70.4	70.4	70.4	71.4	71.4	71.4
Calculated diameter of ND-PG (nm)	6.57	7.70	9.97	10.57	12.60	8.78	9.41	11.46
Calculated thickness of PG (nm)	0.81	1.37	2.42	2.72	3.74	1.82	2.13	3.16
Numbers of glycerol unit (x 10^3) [b]	0.87	1.80	4.59	5.61	10.0	2.90	3.74	7.35
Thickness ratio (DLS/calculated) [c]	6.61	4.79	3.39	3.19	3.06	3.81	3.30	2.84
Volume ratio (DLS/calculated) [c]	22.84	17.53	11.50	10.76	11.71	12.41	9.99	8.91

	ND50(N)-PG(l)	ND50(N)-PG(m)	ND50(A)-PG
PG/ND ratio by TGA	0.69	0.85	1.19
Weight of PG layer (x 10^{-18} g/particle)	103.0	126.9	177.7
Volume of PG (x 10^4 nm^3) [a]	8.17	10.1	14.1
Volume of ND core (x 10^4 nm^3)	4.27	4.27	4.27
Calculated diameter of ND-PG (nm)	61.93	64.92	70.51
Calculated thickness of PG (nm)	9.29	10.79	13.58
Numbers of glycerol unit (x 10^6) [b]	0.837	1.03	1.44
Thickness ratio (DLS/calculated) [c]	0.66	1.02	1.07
Volume ratio (DLS/calculated) [c]	0.58	1.03	1.12

[a] Density of PG layer is assumed to be 1.261 g/cm^3.
[b] Molecular weight of GD is 74.08 (g/mol).
[c] Ratio of the size from DLS in 10 mM NaCl to calculated value.

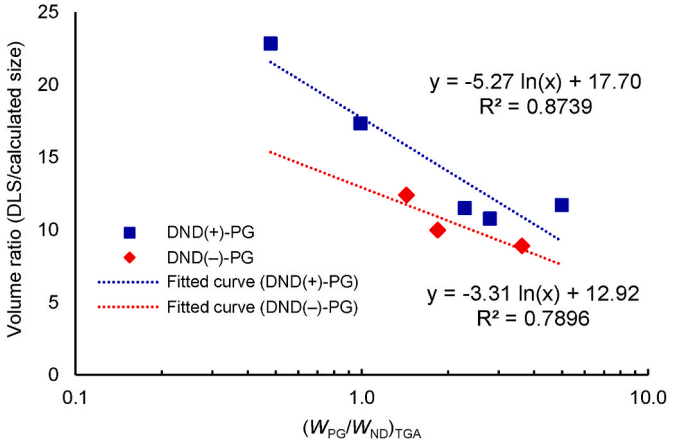

Fig. 9. Relationship between the PG/ND weight ratio and the volume increase ratio of PG layer of compact structure (calculated) to the expanded structure (in 10 mM NaCl) of DND-PGs. (A colour version of this figure can be viewed online.)

median hydrodynamic diameter measured by DLS (D_{50}, number basis) was 3.89 nm.

4.4. Water dispersion of ζ-negative DND (DND(−))

DND powder was annealed in O_2/N_2 (4/96 (v/v)) at 420 °C for 2 h. Resulting powder was suspended in water (3.0%) and pH was adjusted to 10.5, and then agitated vigorously with ZrO_2 beads (30 μmφ) at the tip speed of 8 m/s for 2 h. ZrO_2 beads were removed by decantation and then, centrifuged at 20000*g* for 10 min to give black dispersion. The median hydrodynamic diameter measured by DLS (D_{50}, number basis) was 4.44 nm.

4.5. DND(+)-PG(xl)

An aqueous dispersion of ζ-positive DND was evaporated to dryness. The solid residue was dried at 105 °C for 2 h. To a suspension of resulting DND powder (0.50 g) in ethylene glycol (15.0 g), GD (11.3 g, 0.152 mol) was added dropwise over 1.5 h to keep the temperature in the range of 93–109 °C. The resulting black dispersion was stirred at the same temperature overnight. After the reaction was cooled below 40 °C, water (40 mL) was added slowly to degrade the unreacted GD. The dispersion was diluted with water to ca. 400 mL and concentrated with ultrafiltration membrane (Ultracel® membrane, 100 kDa) to < 40 mL. The concentrate was diluted and concentrated again, which was repeated five times, and the weight of resulting black water dispersion was adjusted to 50.0 g with water. To remove free PG, 40.0 g of water dispersion was ultra-centrifuged at 183400*g* (50000 rpm) for 2 h. Supernatant (80–90% of total amount) was removed carefully and remained lower layer was diluted with water, and ultra-centrifuged again, which was repeated four times (The centrifugation time ranged 1.5–2.5 h). The resulting lower layer was adjusted to 40.0 g with water. An aliquot of the dispersion was accurately weighed (3.0153 g) and dried on heated PTFE sheet. From the weight of the residue (0.0417 g), the sample concentration was determined to be 1.38% (w/w). The net yield of DND(+)-PG(xl) was 0.55 g from 0.40 g of DND.

FT-IR (DRIFT with KBr, cm^{-1}): 3332, 2918, 2875, 1458, 1118, 1078 (C–O). ^{1}H NMR (500 MHz, D_2O): δ ppm 3.42, 3.50, 3.58, 3.75, 3.88. The results of TGA (Air atmosphere, 20 °C/min) and elemental analysis are in Tables S2–1 and S2–2, respectively.

DND(+)-PG(l) and DND(+)-PG(h) were prepared as the same manner except for the quantity of reagents was changed according to the values in Table 1 as the quantitative ratio. Yield of DND(+)-PG(h) was 0.17 g from 0.10 g of DND (corresponds to the size of ultra-centrifugation). Yield of DND(+)-PG(h) was 3.06 g from 1.01 g of DND.

4.6. DND(+)-PG(xh)

DND powder prepared by above procedure (0.25 g) was suspended in GD (5.0 mL = 5.57 g, 0.075 mol). After DND was dispersed to result a black dispersion, GD (10.0 mL, 0.15 mol) was additionally added. The reaction was stirred at 140 °C for 6.5 h. Purification was done in the same manner as DND(+)-PG(xl). Yield (net) 1.58 g.

4.7. DND(−)-PG(m)

To an aqueous dispersion of ζ-negative DND, 1 M HCl was added to adjust pH to about 3.5. The resulting precipitate was collected by centrifugation at 30000*g* for 30 min. The precipitate was washed with water once and dried at 70 °C *in vacuo* overnight, then at 120 °C for 4 h. Using the resulting DND powder, sample was prepared in the same manner as DND(+)-PG samples. The net yield of DND(−)-PG was 1.18 g from 0.50 g of DND.

DND(−)-PG(h) and DND(−)-PG(l) were prepared as the same manner except for the quantity of reagents was changed according to the values in Table 1 as the quantitative ratio. Yield of DND(−)-PG(h) was 0.91 g from 0.25 g of DND, and DND(−)-PG(l) was 0.52 g from 0.25 g of DND.

4.8. ND50(A)-PG

ND50 (0.20 g, MD50 from Tomei Diamond) was treated with a mixture of conc-H_2SO_4 (15.0 mL) and HNO_3 (70%, 5.0 mL) at 150 °C for 5 h. The treatment mixture was poured into 200 mL of water, and centrifuged (20000*g*, 10 min). Precipitate was washed with water twice (40 mL and 25 mL) and dried at 105 °C *in vacuo* to give black powder (0.18 g).

The acid treated ND50 (ND50(A), 0.15 g) was dispersed in ethylene glycol (1.03 mL) and heated at 140 °C. GD (16.12 g, 0.218 mol) was added to the dispersion slowly for 1 h, and the reaction was stirred at the same temperature overnight. Work-up and purification was done in the same manner as DND(+)-PG(xl) except for the concentration with ultrafiltration membrane was done only once before the ultracentrifugation. Yield (net) 0.34 g.

DND(N)-PG(m) and DND(N)-PG(l) were prepared by the same procedure but ND50 was just dried at 105 °C *in vacuo* without acid treatment before the reaction (ND50(N)). The net yield of ND50(N)-PG(m) was 0.36 g from 0.20 g of ND50(N), and ND50(N)-PG(l) was 0.41 g from 0.25 g of ND50(N).

4.9. ^{13}C NMR measurement

^{13}C NMR measurements were done in 5 mmφ tube at the ND-PG concentration of approx. 20% in D_2O except for ND50(N)-PG(m) and ND50(N)-PG(l) that were measured at 10% and 15%, respectively. All measurements were done at 30 °C. Chemical shift of diamond core was adjusted to 36.3 ppm at the peak top as a reference.

Funding

Naoki Komatsu reports financial support was provided by Japan Society for the Promotion of Science. Masahiro Nishikawa has patent pending to Daicel Co.

CRediT authorship contribution statement

Masahiro Nishikawa: Conceptualization, Methodology, Validation, Formal analysis, Investigation, Writing – original draft, Project administration. **Ming Liu:** Methodology, Validation, Investigation. **Taro Yoshikawa:** Methodology, Validation. **Hidekazu Takeuchi:** Investigation. **Naoyoshi Matsuno:** Investigation. **Naoki Komatsu:** Conceptualization, Writing – review & editing, Supervision, Project administration, Funding acquisition.

Declaration of competing interest

The authors declare that they have no known competing financial interests or personal relationships that could have appeared to influence the work reported in this paper.

Data availability

Data will be made available on request.

Acknowledgement

We acknowledge Mr. Shougang He, Mr. Hideo Yagasaki, Mr. Yusuke Okamoto, Mr. Takashi Kouchi and Mr. Shingo Himeda (Daicel Corporation, Japan) for their helpful discussion and experimental help in NMR, BET-SSA and viscosity measurements. We also thank Dr. Yajuan Zou (Okayama University, Japan), Prof. Md. Mahbubor Rahman (University of Rajshahi, Bangladesh), Mr. Yuya Miyake (Hosei University, Japan), Dr. Xiaoxiao Chen and Ms. Jie Yu (Kyoto University, Japan) for useful information and discussion about PG functionalization. This work was partly supported by JSPS KAKENHI (20H02584 and 21K19906).

Appendix A. Supplementary data

Supplementary data to this article can be found online at https://doi.org/10.1016/j.carbon.2023.01.025.

References

[1] L. Zhao, T. Takimoto, M. Ito, N. Kitagawa, T. Kimura, N. Komatsu, Chromatographic separation of highly soluble diamond nanoparticles prepared by polyglycerol grafting, Angew. Chem. Int. Ed. 50 (2011) 1388–1392, https://doi.org/10.1002/anie.201006310.

[2] Y. Zou, N. Komatsu, Quantitative investigation of the interaction between proteins and charged functional groups on the polyglycerol-grafted nanodiamond surface, Carbon 163 (2020) 395–401, https://doi.org/10.1016/j.carbon.2020.02.089.

[3] Y. Zou, S. Ito, F. Yoshino, Y. Suzuki, L. Zhao, N. Komatsu, Polyglycerol grafting shields nanoparticle from protein corona formation to avoid macrophage uptake, ACS Nano 14 (2020) 7216–7226, https://doi.org/10.1021/acsnano.0c02289.

[4] T. Jafari, A. Simchim, N. Khakpash, Synthesis and cytotoxicity assessment of superparamagnetic iron–gold core–shell nanoparticles coated with polyglycerol, J. Colloid Interface Sci. 345 (2010) 64–71, https://doi.org/10.1016/j.jcis.2010.01.038.

[5] L. Zhou, C. Gao, W. Xu, Efficient grafting of hyperbranched polyglycerol from hydroxyl-functionalized multiwalled carbon nanotubes by surface-initiated anionic ring-opening polymerization, Macromol. Chem. Phys. 210 (2009) 1011–1018, https://doi.org/10.1002/macp.200900134.

[6] L. Zhou, C. Gao, W. Xu, X. Wang, Y. Xu, Enhanced biocompatibility and biostability of CdTe quantum dots by facile surface-initiated dendritic polymerization, Biomacromolecules 10 (2009) 1865–1874, https://doi.org/10.1021/bm9002877.

[7] N. Komatsu, Poly(glycerol)-based biomedical nanodevices constructed by functional programming on inorganic nanoparticles for cancer nanomedicine, Acc. Chem. Res. 56 (2023) 106–116, https://doi.org/10.1021/acs.accounts.2c00615.

[8] L. Zhao, T. Chano, S. Morikawa, Y. Saito, A. Shiino, S. Shimizu, T. Maeda, T. Irie, S. Aonuma, H. Okabe, T. Kimura, T. Inubushi, N. Komatsu, Hyperbranched polyglycerol-grafted superparamagnetic iron oxide nanoparticles: synthesis, characterization, functionalization, size separation, magnetic properties, and biological applications, Adv. Funct. Mater. 22 (2012) 5107–5117, https://doi.org/10.1002/adfm.201201060.

[9] H. Qin, K. Maruyama, T. Amano, T. Murakami, N. Komatsu, Hyperbranched polyglycerol-grafted titanium oxide nanoparticles: synthesis, derivatization, characterization, size separation, and toxicology, Mater. Res. Express 3 (2016), 105049, https://doi.org/10.1088/2053-1591/3/10/105049.

[10] Y. Wang, G. Reina, H.G. Kang, X. Chen, Y. Zou, Y. Ishikawa, M. Suzuki, N. Komatsu, Polyglycerol functionalized ^{10}B enriched boron carbide nanoparticle as an effective bimodal anticancer nanosensitizer for boron neutron capture and photothermal therapies, Small 18 (2022), 2204044, https://doi.org/10.1002/smll.202204044.

[11] B.S. Miller, L. Bezinge, H.D. Gliddon, D. Huang, G. Dold, E.R. Gray, J. Heaney, P. J. Dobson, E. Nasatouli, J.J.L. Morton, R.A. McKendry, Spin-enhanced nanodiamond biosensing for ultrasensitive diagnostics, Nature 587 (2020) 588–593, https://doi.org/10.1038/s41586-020-2917-1.

[12] L.P. Suarez-Kelly, S.H. Sun, C. Ren, I.V. Rampersaud, D. Albertson, M.C. Duggan, T. C. Noel, N. Courtney, N.J. Buteyn, C. Moritz, L. Yu, V.O. Yildiz, J.P. Butchar, S. Tridandapani, A.A. Rampersaud, W.E. Carson, Antibody conjugation of fluorescent nanodiamonds for targeted innate immune cell activation, ACS Appl. Nano Mater. 4 (2021) 3122–3139, https://doi.org/10.1021/acsanm.1c00256.

[13] S. Sotoma, R. Igarashi, J. Iimura, Y. Kumiya, H. Tochio, Y. Harada, M. Shirakawa, Suppression of nonspecific protein-nanodiamond adsorption enabling specific targeting of nanodiamonds to biomolecules of interest, Chem. Lett. 44 (2015) 354–356, https://doi.org/10.1246/cl.141036.

[14] D. Terada, T. Genjo, T.F. Segawa, R. Igarashi, M. Shirakawa, Nanodiamonds for bioapplications–specific targeting strategies, Biochim. Biophys. Acta Gen. Subj. 1864 (2020), 129354, https://doi.org/10.1016/j.bbagen.2019.04.019.

[15] D. Terada, S. Sotoma, Y. Harada, R. Igarashi, M. Shirakawa, One-pot synthesis of highly dispersible fluorescent nanodiamonds for bioconjugation, Bioconjugate Chem. 29 (2018) 2786–2792, https://doi.org/10.1021/acs.bioconjchem.8b00412.
[16] M. Fujiwara, S. Sun, A. Dohms, Y. Nishimura, K. Suto, Y. Takezawa, K. Oshimi, L. Zhao, N. Sadzak, Y. Umehara, Y. Teki, N. Komatsu, O. Benson, Y. Shikano, E. Kage-Nakadai, Real-time nanodiamond thermometry probing in vivo thermogenic responses, Sci. Adv. 6 (2020), eaba9636., https://doi.org/10.1126/sciadv.aba9636.
[17] M. Fujiwara, G. Uchida, I. Ohki, M. Liu, A. Tsurui, T. Yoshikawa, M. Nishikawa, N. Mizuochi, All-optical nanoscale thermometry based on silicon-vacancy centers in detonation nanodiamonds, Carbon 198 (2022) 57–62, https://doi.org/10.1016/j.carbon.2022.06.076.
[18] F. Yoshino, T. Amano, Y. Zou, J. Xu, F. Kimura, Y. Furusho, T. Chano, T. Murakami, L. Zhao, N. Komatsu, Preferential tumor accumulation of polyglycerol functionalized nanodiamond conjugated with cyanine dye leading to near-infrared fluorescence in vivo tumor imaging, Small 15 (2019), 1901930, https://doi.org/10.1002/smll.201901930.
[19] F.-J. Hsieh, S. Sotoma, H.-H. Lin, C.-Y. Cheng, T.-Y. Yu, C.-L. Hsieh, C.-H. Lin, H.-C. Chang, Bioorthogonal Fluorescent nanodiamonds for continuous long-term imaging and tracking of membrane proteins, ACS Appl. Mater. Interfaces 11 (2019) 19774–19781, https://doi.org/10.1021/acsami.9b03640.
[20] K. Kvakova, M. Ondra, J. Schimer, M. Petrik, Z. Novy, H. Raabova, M. Hajduch, P. Cigler, Visualization of sentinel lymph nodes with mannosylated fluorescent nanodiamonds, Adv. Funct. Mater. 32 (2022), 2109960, https://doi.org/10.1002/adfm.202109960.
[21] J. Barton, M. Gulka, J. Tarabek, Y. Mindarava, Z. Wang, J. Schimer, H. Raabova, J. Bednar, M.B. Plenio, F. Jelezko, M. Nesladek, P. Cigler, Nanoscale dynamic readout of a chemical redox process using radicals coupled with nitrogen-vacancy centers in nanodiamonds, ACS Nano 14 (2020) 12938–12950, https://doi.org/10.1021/acsnano.0c04010.
[22] J.-P. Boudou, M.-O. David, V. Joshi, H. Eidi, P.A. Curmi, Hyperbranched polyglycerol modified fluorescent nanodiamond for biomedical research, Diam. Relat. Mater. 38 (2013) 131–138, https://doi.org/10.1016/j.diamond.2013.06.019.
[23] L. Zhao, A. Shiino, H. Qin, T. Kimura, N. Komatsu, Synthesis, characterization, and magnetic resonance evaluation of polyglycerol-functionalized detonation nanodiamond conjugated with gadolinium(III) complex, J. Nanosci. Nanotechnol. 15 (2015) 1076–1082, https://doi.org/10.1166/jnn.2015.9738.
[24] L. Zhao, Y. Nakae, H. Qin, T. Ito, T. Kimura, H. Kojima, L. Chan, N. Komatsu, Polyglycerol-functionalized nanodiamond as a platform for gene delivery: derivatization, characterization, and hybridization with DNA, Beilstein J. Org. Chem. 10 (2014) 707–713, https://doi.org/10.3762/bjoc.10.64.
[25] L. Zhao, Y.H. Xu, H. Qin, S. Abe, T. Akasaka, T. Chano, F. Watari, T. Kimura, N. Komatsu, X. Chen, Platinum on nanodiamond: a promising prodrug conjugated with stealth polyglycerol, targeting peptide and acid-responsive antitumor drug, Adv. Funct. Mater. 24 (2014) 5348–5357, https://doi.org/10.1002/adfm.201304298.
[26] M. Nishikawa, H.G. Kang, Y. Zou, H. Takeuchi, N. Matsuno, M. Suzuki, N. Komatsu, Conjugation of phenylboronic acid moiety through multistep organic transformations on nanodiamond surface for an anticancer nanodrug for boron neutron capture therapy, Bull. Chem. Soc. Jpn. 94 (2021) 2302–2312, https://doi.org/10.1246/bcsj.20210200.
[27] S. Sotoma, Polyglycerol/Polydopamine-coated nanoparticles for biomedical applications, Front. Mater. 9 (2022), 878455, https://doi.org/10.3389/fmats.2022.878455.
[28] Z. Rafiee, S. Omidi, Modification of carbon-based nanomaterials by polyglycerol: recent advances and applications, RSC Adv. 12 (2022) 181–192, https://doi.org/10.1039/D1RA07554C.
[29] Y. Wu, T. Weil, Recent developments of nanodiamond quantum sensors for biological applications, Adv. Sci. 9 (2022), 2200059, https://doi.org/10.1002/advs.202200059.
[30] A. Mzyk, Y. Ong, A.R.O. Moreno, S.K. Padamati, Y. Zhang, C.A. Reyes-San-Martin, R. Schirhagl, Diamond color centers in diamonds for chemical and biochemical analysis and visualization, Anal. Chem. 94 (2022) 225–249, https://doi.org/10.1021/acs.analchem.1c04536.
[31] M.B.A. Olia, P.S. Donnelly, L.C.L. Hollenberg, P. Mulvaney, D.A. Simpson, Advances in the surface functionalization of nanodiamonds for biological applications: a review, ACS Appl. Nano Mater. 4 (2021) 9985–10005, https://doi.org/10.1021/acsanm.1c02698.
[32] H.-S. Jung, K.C. Neuman, Surface modification of fluorescent nanodiamonds for biological applications, Nanomaterials 11 (2021) 153, https://doi.org/10.3390/nano11010153.
[33] A. Sunder, R. Hanselmann, H. Frey, R. Mu, Controlled synthesis of hyperbranched polyglycerols by ring-opening multibranching polymerization, Macromolecules 32 (1999) 4240–4246, https://doi.org/10.1021/ma990090w.
[34] D. Wilms, J. Nieberle, J. Klos, H. Löwe, H. Frey, Synthesis of hyperbranched polyglycerol in a continuous flow microreactor, Chem. Eng. Technol. 30 (2007) 1519–1524, https://doi.org/10.1002/ceat.200700277.
[35] S. Xiaoying, Y. Xiaohui, L. Yunhang, W. Xinling, Synthesis and characterization of a multiarm star polymer, J. Polym. Sci. Polym. Chem. 42 (2004) 2356–2364, https://doi.org/10.1002/pola.20083.
[36] E. Mohammadifar, A. Bodaghi, A. Dadkhahtehrani, A.N. Kharat, M. Adeli, R. Haag, Green synthesis of hyperbranched polyglycerol at room temperature, ACS Macro Lett. 6 (2017) 35–40, https://doi.org/10.1021/acsmacrolett.6b00804.
[37] T. Yoshikawa, M. Liu, S.L.Y. Chang, I.C. Kuschnerus, Y. Makino, A. Tsurui, T. Mahiko, M. Nishikawa, Steric interaction of polyglycerol-functionalized detonation nanodiamonds, Langmuir 38 (2022) 661–669, https://doi.org/10.1021/acs.langmuir.1c02283.
[38] S. Osswald, G. Yushin, V. Mochalin, S.O. Kucheyev, Y. Gogotsi, Control of sp2/sp3 carbon ratio and surface chemistry of nanodiamond powders by selective oxidation in air, J. Am. Chem. Soc. 128 (2006) 11635–11642, https://doi.org/10.1021/ja063303n.
[39] M. Kurzyp, H.A. Girard, Y. Cheref, E. Brun, C. Sicard-Roselli, S. Saada, J.-C. Arnault, Hydroxyl radical production induced by plasma hydrogenated nanodiamonds under X-ray irradiation, Chem. Commun. 53 (2017) 1237–1240, https://doi.org/10.1039/C6CC08895C.
[40] C.H. Klute, W. Viehmann, Heat of polymerization of phenyl glycidyl ether and of an epoxy resin, J. Appl. Polym. Sci. 5 (1961) 86–95, https://doi.org/10.1002/app.1961.070051313.
[41] A.M. Panich, A.I. Shames, N.A. Sergeev, M. Olszewski, J.K. McDonough, V. N. Mochalin, Y. Gogotsi, Nanodiamond graphitization: a magnetic resonance study, J. Phys. Condens. Matter 25 (2013), 245303, https://doi.org/10.1088/0953-8984/25/24/245303.
[42] X.W. Fang, J.D. Mao, E.M. Levin, K. Schmidt-Rohr, Nonaromatic Core-shell structure of nanodiamond from solid-state NMR spectroscopy, J. Am. Chem. Soc. 131 (2009) 1426–1435, https://doi.org/10.1021/ja8054063.
[43] C. Bradac, T. Gaebel, N. Naidoo, M.J. Sellars, J. Twamley, L.J. Brown, A.S. Barnard, T. Plakhotnik, A.V. Zvyagin, J.R. Rabeau, Observation and control of blinking nitrogen-vacancy centres in discrete nanodiamonds, Nat. Nanotechnol. 5 (2010) 345–349, https://doi.org/10.1038/nnano.2010.56.
[44] W. Radke, G. Litvinenko, A.H.E. Müller, Effect of core-forming molecules on molecular weight distribution and degree of branching in the synthesis of hyperbranched polymers, Macromolecules 31 (1998) 239–248, https://doi.org/10.1021/ma970952y.
[45] M. Tomšič, M. Bešter-Rogač, A. Jamnik, W. Kunz, D. Touraud, A. Bergmann, O. Glatter, Nonionic surfactant Brij 35 in water and in various simple alcohols: structural investigations by small-angle X-ray scattering and dynamic light scattering, J. Phys. Chem. B 108 (2004) 7021–7032, https://doi.org/10.1021/jp049941e.
[46] ISO 22412:2017, Particle Size Analysis – Dynamic Light Scattering (DLS).
[47] Y. Zou, M. Nishikawa, N. Komatsu, Organic chemistry for nanodiamond: controlled functionalization, quantitative characterization and structure-property relationships, Carbon Reports 1 (2022) 70–78, https://doi.org/10.7209/carbon.010204.
[48] S. Sotoma, R. Igarashi, M. Shirakawa, Moderate plasma treatment enhances the quality of optically detected magnetic resonance signals of nitrogen-vacancy centres in nanodiamonds, Appl. Phys. A 122 (2016) 522, https://doi.org/10.1007/s00339-016-0030-y.
[49] I. Rehor, P. Cigler, Precise estimation of HPHT nanodiamond size distribution based on transmission electron microscopy image analysis, Diam. Relat. Mater. 46 (2014) 21–24, https://doi.org/10.1016/j.diamond.2014.04.002.
[50] P. Reineck, L.F. Trindade, J. Havlik, J. Stursa, A. Heffernan, A. Elbourne, A. Orth, M. Capelli, P. Cigler, D.A. Simpson, B.C. Gibson, Not all fluorescent nanodiamonds are created equal: a comparative study, Part. Part. Syst. Char. 36 (2019), 1900009, https://doi.org/10.1002/ppsc.201900009.